Sensors and Materials, Vol. 36, No. 11 (2024) 4815–4833
MYU Tokyo

S & M 3833

Tool Wear Classification Based on Support Vector Machine and Deep Learning Models

Yung-Hsiang Hung, Mei-Ling Huang, Wen-Pai Wang,* and Hsiao-Dan Hsieh

Department of Industrial Engineering and Management, National Chin-Yi University of Technology,
No. 57, Sec. 2, Zhongshan Rd., Taiping Dist., Taichung 41170, Taiwan, R.O.C.

(Received June 25, 2024; accepted October 21, 2024)

Keywords: tool wear, machine vision, image classification, support vector machine, convolutional neural network

Tool status is crucial for maintaining workpiece quality during machine processing. Tool wear, an inevitable occurrence, can degrade the workpiece surface and even cause damage if it becomes severe. In extreme cases, it can also shorten the machine tool service life. Therefore, accurately assessing tool wear to avoid unnecessary production costs is essential. We present a wear classification model using machine vision to analyze tool images. The model categorizes wear images on the basis of predefined wear levels to assess tool life. The research involves capturing images of the tool from three angles using a digital microscope, followed by image preprocessing. Wear measurement is performed using three methods: gray-scale value, gray-level co-occurrence matrix, and area detection. The K-means clustering technique is then applied to group the wear data from these images, and the final wear classification is determined by analyzing the results of the three methods. Additionally, we compare the recognition accuracies of two models: support vector machine (SVM) and convolutional neural network (CNN). The experimental results indicate that, within the same tool image sample space, the CNN model achieves an accuracy of more than 93% in all three directions, whereas the accuracy of the SVM model, affected by the number of samples, has a maximum of only 89.8%.

1. Introduction

Precision machining technology is essential in modern manufacturing, especially given the rising demand for equipment and components in aerospace, automotive, and precision machinery sectors. The advancement of processing technology is therefore crucial. Precision machining is extensively employed in micro- and ultra-precision equipment owing to its exceptional ability to process various materials and complex three-dimensional surfaces. However, the challenges posed by ultra-high-speed intermittent cutting and the use of micro-tools mean that tool wear—referring to the gradual deterioration of cutting tools in processes such as milling, turning, and drilling—can significantly affect workpiece quality. Tool wear impacts tool life, workpiece

*Corresponding author: e-mail: wangwp@ncut.edu.tw
https://doi.org/10.18494/SAM5205

ISSN 0914-4935

dimensional accuracy, surface finish, and the efficiency of automated production operations. It can lead to defects in parts, increased production costs, and unexpected machine downtimes.

Previous research has consistently shown that an early and effective detection of tool wear can prevent machine damage, avoid unplanned shutdowns, and minimize workpiece scrapping. This leads to significant improvements in manufacturing quality and cost reduction.(1–3) Zhou and Xue highlighted that traditional tool wear monitoring methods rely on periodic inspections and manual measurements based on the operator's experience, which can be both time-consuming and inaccurate.(4) As a result, effective tool wear monitoring has become a crucial focus in ultraprecision machining. There is a need for tool condition monitoring systems that can continuously and accurately manage tool wear to minimize downtime and enhance product quality. In response to this need, Singh *et al.* proposed an automated detection system for high-performance machining environments, utilizing various sensors, modeling techniques, and data analysis methods to assess cutting tool wear.(5)

In recent years, the rapid advancements in IoT and big data technologies have made the application of machine learning (ML) to production quality and machine preventive maintenance (PM) increasingly significant in modern manufacturing. By analyzing large volumes of production data, ML can substantially enhance production efficiency and product quality while reducing maintenance costs.(6–7) Concurrently, the growth of AI has led researchers to apply data-driven methods for developing pattern recognition algorithms to predict tool wear.(8) These methods typically involve extracting feature variables from sensor data and processing signals to predict tool wear. Various classification algorithms are used for this purpose, including artificial neural networks (ANNs), fuzzy logic, pattern recognition, support vector machines (SVMs), decision trees, K-nearest neighbor classifiers (KNNs), adaptive neuro-fuzzy inference systems (ANFISs), Bayesian networks (BNs), principal component analysis (PCA), and convolutional neural networks (CNNs). The effectiveness of these methods depends on how well the extracted features correlate with the tool wear status.(9–12) The accurate prediction of tool wear can significantly improve production efficiency and quality by facilitating timely tool replacement, thus preventing production line interruptions and losses. For instance, Bagga *et al.* investigated the use of ANNs to predict cutting force and vibration related to tool wear during the turning process.(13) Their study, based on Taguchi L_9 experiments using alloy inserts and EN-8 medium carbon steel, demonstrated that ANNs can effectively predict tool wear, thus offering a valuable tool for monitoring and managing tool condition.

Deep learning, an advanced data analysis technique evolved from traditional neural networks, has recently been applied to tool condition monitoring. In machining processes, time-series images combined with deep learning methods are utilized to classify and predict tool wear effectively.(14) Serin *et al.* conducted research on applying deep learning for tool wear analysis and damage reduction, with the goal of accurately predicting tool wear and preventing adverse conditions for cutting tools and machinery.(11) Deep learning technologies can model complex, previously unexamined functional relationships and offer exceptional adaptability and self-learning capabilities, which help mitigate the effects of external interferences during machining. However, current deep learning approaches to tool wear monitoring face challenges, including difficulties in interpreting extracted features and inability to fully account for the significance of different feature maps, which can limit prediction accuracy.(15–17)

In this study, we employ a machine vision system to analyze tool wear from three perspectives: corner wear, flank wear, and crater wear (see Fig. 1). After capturing and preprocessing the images, the wear is assessed using three distinct methods. The processed images are analyzed to extract feature values indicative of tool wear. The K-means clustering technique is then applied to categorize the degree of wear of each sample. The results from these three methods are compared to determine the final wear classification and evaluate the effectiveness of each approach. We also aim to compare the wear image classification accuracies of SVMs and CNNs to determine their ability to accurately classify tool wear across different samples. The accurate real-time detection of tool status could prevent losses associated with delayed tool replacement, thereby significantly enhancing the overall factory processing efficiency. The specific objectives of this study are as follows.

1. Calculate wear areas using processed images to establish wear level grading data.
2. Construct a model to achieve optimal wear level recognition.

2. Literature Review

2.1 Definition of tool wear

In machining processes, tool wear refers to the gradual failure of cutting tools as a result of frequent operation. During cutting, the tool comes into contact with the workpiece and chips, causing intense friction. This continuous wear is induced by high temperatures and friction, with the extent of wear varying depending on shape, depth, cutting fluid, and cutting speed. Consequently, the sharpness and efficiency of the tool are affected. This phenomenon is unavoidable and can be considered normal dulling, but it also leads to issues such as increased workpiece surface roughness, higher cutting forces, rising cutting temperatures, reduced machining precision, and shorter tool life. Generally, tool wear manifests in various forms (e.g., flank wear, crater wear, and chipping). These wear patterns primarily depend on the tool characteristics, workpiece material, cutting conditions, and machining techniques. Under normal machining conditions, flank wear is the most common and significant wear. Flank wear width (VB) is the most crucial parameter for assessing tool life.[18]

Tool life can be divided into three stages, as shown in Fig. 2. These stages provide an effective means to predict and manage the lifespan of cutting tools, thereby avoiding unnecessary production costs and time loss.[17]

1. Break-in Region: This stage spans from point A to point B in Fig. 2 and is known as the rapid initial wear period. During this phase, the tool wear rate is relatively high because of the

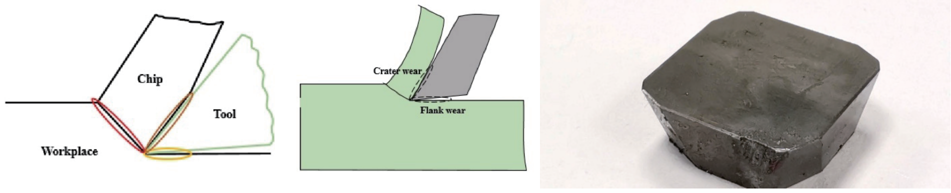

Fig. 1. (Color online) Schematic diagram of tool wear.

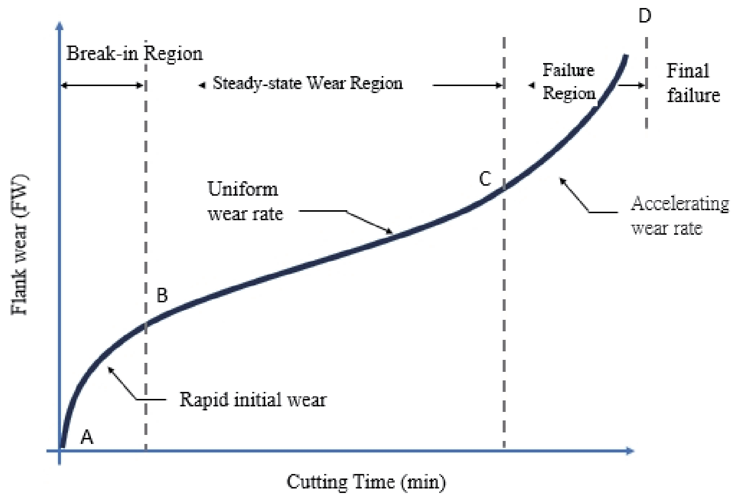

Fig. 2. (Color online) Tool life curve.

initial interaction between the tool surface and the workpiece. The wear is primarily due to the abrasion of microscopic surface irregularities and eventually enters a relatively stable state.

2. Steady-state Wear Region: This stage extends from point B to point C and is characterized by a relatively stable and uniform wear rate. This is the main working period of the tool and the longest stage of its usage. During this phase, the wear rate is low and stable, allowing the tool to maintain good machining quality.
3. Failure Region: This stage runs from point C to point D, where the tool enters an accelerated wear period. The wear rate increases significantly because the tool has worn to its limit, causing wear to intensify. During this phase, the tool performance rapidly declines, ultimately leading to failure, as indicated by point D. At this point, the tool can no longer be used and must be replaced to ensure machining quality and efficiency.

2.2 Tool wear detection

In the early stages of technological development, the majority of research on tool wear relied on empirical rules and experimental data to determine the wear state of tools. Dornfeld and Kannatey-Asibu classified tool wear detection techniques into two categories: direct techniques and indirect techniques.[19] Indirect techniques use sensor signals to output parameters related to wear status during cutting operations and predict tool wear using these parameters. The drawback of this approach is that the measured parameters are susceptible to environmental effects and do not directly quantify tool wear. Bao and Tansel conducted research on tool wear in vertical milling cutter grooves using mild steel and aluminum materials.[20] They estimated tool wear by monitoring the cutting force in the workpiece feed direction and dynamically adjusted cutting parameters to control the cutting force, thereby extending the tool life. Rmili *et al.* used a three-axis accelerometer to measure vibration characteristics during turning and proposed an average power analysis technique to extract indicative parameters from the vibration response, which describes the tool condition throughout its lifespan.[21]

In contrast, direct techniques offer advantages in accuracy and reliability.[22] Direct techniques use optical, radioactive, and resistive proximity sensors, or vision systems to directly measure the actual geometric changes in tools. Machine vision detection technology overcomes the difficulty of contact between the tool and the workpiece during cutting due to the presence of coolant, making the measurement of tool geometry and dimensional changes more accurate. Compared with indirect techniques, machine vision does not require complex measurement systems, is more flexible, and is cost-effective. In micro–milling processes, tool wear conditions are critical to product geometry and surface integrity. Zhu and Yu proposed a novel tool wear surface area monitoring method based on complete tool wear images.[23] Unlike the traditional tool wear width standard, this method better reflects the tool condition. They introduced a region-growing algorithm based on morphological component analysis (MCA) to solve the tool wear problem by decomposing the original micro–milling-tool image into target tool, background, and noise images to extract effective tool wear areas. Results showed that the wear surface area better reflects the tool usage status than do traditional tool wear width standards. However, direct techniques using machine vision for tool wear detection also have significant limitations. Different optical sensors, such as lasers, CCD and CMOS cameras, and thermal infrared cameras, exhibit considerable variability in image quality.[24]

2.3 Cutting tool wear prediction

As the demands of Industry 4.0 continue to grow, precision machining plays a crucial role in modern manufacturing. Tool wear is a major factor affecting product quality, production time, and manufacturing costs. Therefore, assessing and accurately predicting tool wear before significant damage occurs to the workpiece are essential for ensuring high-quality workpieces and reducing production costs.[25] In recent years, many researchers have applied data acquisition and signal processing methods to evaluate tool wear.[26] Kara utilized Taguchi quality engineering in machining experiments to minimize tool wear and surface roughness.[27] Dastres and Soori proposed a network-based decision support system using data warehouse management to address tool replacement decisions.[28]

Pimenov *et al.* combined traditional sensor systems with neuro-AI methods to monitor turning tool conditions, replacing decision-making based on human experience.[29] Wang *et al.* integrated IoT sensors and SVM methods to predict tool wear, thereby enhancing the reliability of manufacturing systems.[30] Xu *et al.* introduced an incremental cost-sensitive SVM (ICSSVM) learning model to predict tool breakage in milling operations.[31] Their results showed that even with imbalanced datasets, the prediction accuracy was higher than that of traditional batch cost-sensitive SVM models.

CNN is a multilayer feedforward ANN initially developed to handle two-dimensional image classification problems. Image classification distinguishes different target categories on the basis of image features. An image classification system mainly comprises image information acquisition, information processing, feature extraction, and classification. Generally, image classification involves feature learning to describe the entire image, followed by the use of a classifier to determine the category of the target. This technology has been widely used in facial recognition, vehicle identification, pathological image recognition, and tool monitoring.(32) Chen *et al.* proposed a CNN based on an attention mechanism and bidirectional LSTM networks for monitoring tool wear conditions.(33)

3. Methods

Automated optical inspection (AOI) is a quality inspection method for automated manufacturing vision systems and is characterized as a noncontact testing method. In recent years, AOI has been extensively applied in advanced manufacturing processes to detect potential defects. Image quality inspection is a method used in manufacturing and production processes to assess and ensure the quality of products or workpieces. Through an image inspection system, various defects, such as cracks, dents, and foreign objects, can be detected on products or workpieces. Additionally, the system can accurately measure their dimensions and geometric features to ensure compliance with specifications. AOI machines can detect error features based on standard samples. The most challenging part of detection lies in the effects of variations in brightness and colors. In particular, the image features of the same component type can differ under varying brightness and color conditions. Consequently, image quality inspection identifies different types of products or workpieces and classifies them on the basis of preset standards while recording the data obtained during the inspection process for subsequent analysis and traceability. This process typically includes image capture, image processing, feature extraction, inspection analysis, and result presentation. By integrating these functions and methods, image quality inspection helps improve production efficiency and product yield, ensuring product quality. Image preprocessing involves a series of steps performed on images before recognition to enhance image quality and improve the accuracy and efficiency of subsequent recognition tasks. Image preprocessing includes binarization, image enhancement, image segmentation, and morphological processing.(34) The powerful algorithms of deep CNNs have demonstrated outstanding performance in the field of computer vision. Numerous research groups have proposed training models that combine AOI systems with CNNs for defect detection.(35)

In this study, we begin with the acquisition of tool wear images. In Step 1, high-magnification CCD equipment is used to capture the original tool wear images. In Step 2, these images undergo preprocessing, including grayscale conversion, filtering, negative processing, edge detection, and binarization. Step 3 involves image feature extraction through methods such as grayscale threshold segmentation, gray level co-occurrence matrix calculation, and area detection to obtain key features of the images. Subsequently, wear clustering based on the extracted features is performed to classify the wear parts in the images. We employ CNNs and SVMs as the two classification methods for model training and testing. Finally, performance evaluation is conducted to determine the accuracy and effectiveness of the models, and an intelligent tool wear automatic classification prediction model is confirmed. The research process is illustrated in Fig. 3.

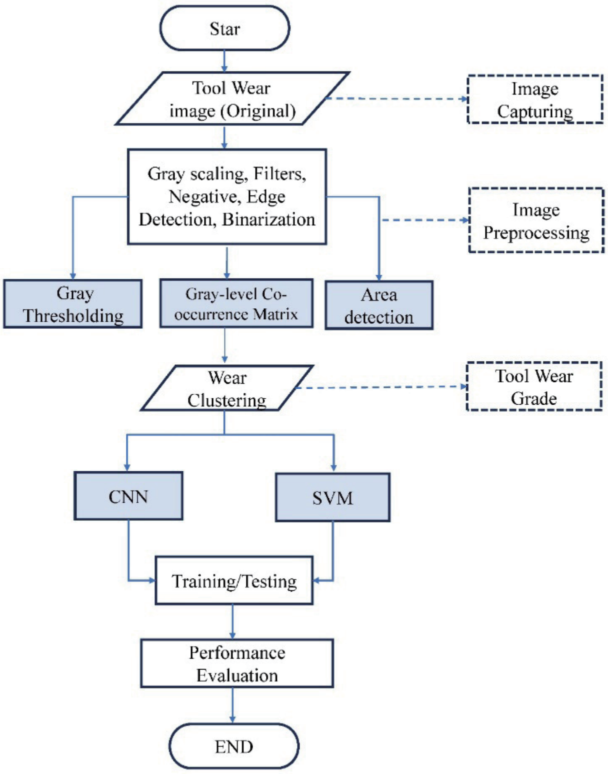

Fig. 3. (Color online) Research process flowchart for the tool wear classification model.

- Image Acquisition: The actual tool edge wear conditions are captured using a digital microscope by fixing the tool in a clamp. The type of tool being measured is a disposable triangular milling insert. Images are captured in three specific directions: 1. corner, 2. minor flank, and 3. major flank. A schematic diagram of the acquisition directions is shown in Fig. 4.
- Wear Measurement Calculation: The captured images, sized at 100 × 100 pixels, are segmented into 10 × 10 pixel blocks. Using MATLAB, the grayscale values of the tool images are calculated. From these, representative feature values, including the maximum and average values, are computed for each of the 100 blocks, as shown in Fig. 5.
- Gray Level Co-occurrence Matrix (GLCM): GLCM is a feature extraction method for processing RGB images.[36] These texture features are calculated by probability, which can be defined as:

$$P_r = C_{ij}(\gamma, \theta), \tag{1}$$

where C_{ij} is the co-occurrence probability between gray levels i and j.

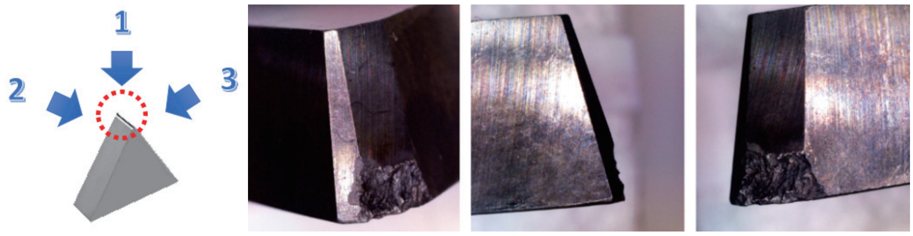

Fig. 4. (Color online) Tool wear of the (1) corner, (2) minor flank, and (3) major flank.

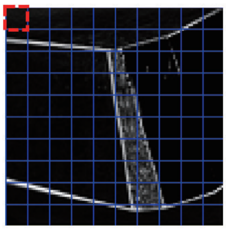

	1	2	3	4	5	6	7	8	9	10
1	23	20	16	16	17	19	18	21	17	13
2	21	21	22	18	20	20	18	20	22	20
3	23	22	23	22	20	21	19	19	16	21
4	22	23	17	21	20	22	21	17	20	22
5	20	20	20	18	18	15	17	21	21	18
6	19	16	20	19	20	18	19	19	19	22
7	13	13	14	14	17	21	16	13	17	17
8	14	16	14	13	11	12	15	17	15	9
9	13	12	10	15	13	11	12	10	12	11
10	10	11	14	16	15	16	12	13	14	15

(a)

	1	2	3	4	5	6	7	8	9	10
1	17.18	16.9	16.74	13.62	10.87	11.37	12.36	11.59	30.15	19.59
2	37.04	39.32	36.44	35.11	30.61	23.3	19.85	23.21	2.39	0.01
3	5.7	6.67	9.1	9.65	43.19	29.6	1.48	9.54	0	0
4	4.99	4.97	4.98	3.74	33.87	38.31	0.02	1.61	0	0
5	4.33	4.98	3.5	3.37	13.23	69.02	7.28	0	0	0
6	3.26	3.71	2.62	3.12	4.17	69.27	27.5	0.02	0	0
7	3.59	3.63	2.77	3.55	4.88	52.67	40.13	0	0	0.09
8	32.63	4.1	4.35	4.2	4.95	45.31	55.68	0.02	0	1.18
9	24.1	48.14	43.85	38.45	28.47	40.78	60.72	20.11	20.4	35.55
10	12.81	13.62	13.96	13.52	17.43	42.9	35.09	27.27	13.78	22.92

(b)

Fig. 5. (Color online) (a) Tool edge wear grayscale matrix. (b) Matrix of degree of tool edge wear.

$$C_{ij} = \frac{P_{ij}}{\sum_{i,j=1}^{G} P_{ij}} \tag{2}$$

Here, P_{ij} represents the number of occurrences of gray levels i and j within the given d, θ, and G values.

We extracted 14 tool feature images from the GLCM, namely, 1. angular second moment, 2. contrast, 3. correlation, 4. sum of squares, 5. inverse difference moment, 6. sum average, 7. sum variance, 8. sum entropy, 9. entropy, 10. difference variance, 11. difference entropy, 12. information measures of correlation I and II, and 13. maximal correlation coefficient.

3.1 Support vector machine

SVM is an ML method based on statistical learning theory. It is theoretically robust, highly adaptable, generalizes well, and has short training times. SVM is primarily used for data classification and finds applications in face detection, image classification, and handwritten recognition. The basic principle of SVM is to find a hyperplane in the feature space that maximizes the margin to separate two classes of data. The following are SVM multiclass classification methods: (1) One-Against-The-Rest where one class of samples is separated from the rest; (2) One-Against-One where every two classes are paired for classification [For N classes, $N(N-1)/2$ SVM classifiers are needed, and the class with the most votes is chosen during testing]; (3) SVM Decision Tree where binary decision trees are combined with SVM to form a multiclass classifier (The drawback is that classification errors can affect subsequent nodes); (4) Multiclass Objective Functions where the objective function is modified to accommodate multiclass needs, but this approach has high computational complexity and is less commonly used. For addressing multiclass problems, we adopt the directed acyclic graph SVMs (DAG-SVMs) proposed by Agarwal *et al.*[37]

Traditional ML methods for image recognition require feature extraction in conjunction with classifiers, enabling algorithms to make predictions using unseen data. Histogram of oriented gradients (HOG) is a feature extraction technique that derives features by accumulating the intensity of gradients in various orientations within image blocks. HOG calculates a histogram of gradient directions for each block and uses it as a feature representation of the block. It divides the image into small regions called "cells." Since HOG features operate on local units of the image, they maintain robustness to both geometric and photometric transformations.[38] The main steps of computing HOG features from an image are as follows.

1. Compute Gradient Magnitude and Orientation: Calculate the gradient of each pixel intensity in both horizontal and vertical directions.
2. Calculate Gradients: Use the G_x and G_y values for each pixel to determine the gradient magnitude and orientation, where the magnitude indicates the edge strength and the orientation indicates the edge direction.

$$\begin{aligned} &\text{Gradientmagnitude:} && \sqrt{G_x^2 + G_y^2} \\ &\text{Gradientangle:} && \tan^{-1}\left(G_y / G_x\right) \end{aligned} \tag{3}$$

SVM is an ML technique aimed at correctly distinguishing different classes of data points by identifying the optimal hyperplane. The process of combining HOG and SVM involves first using HOG to extract features from images, and then inputting these features into the SVM model for image classification.

3.2 Convolutional neural networks

CNNs are a type of deep learning model particularly well suited for image recognition and processing. The advantages of CNNs can be summarized as follows.

- High Image Recognition Capability: CNNs exhibit strong performance in recognizing various image patterns and transformations accurately.
- Effectiveness in Image Classification: In recent years, CNNs have dominated visual recognition competitions, with winners frequently employing CNN architectures.
- Efficient Information Retention: CNNs retain substantial information without excessively increasing the number of parameters, resulting in improved computational speed.

A typical CNN architecture is shown in Fig. 6. The structure and steps of each neural layer are described below.

1. Convolutional Layers: These layers utilize multiple filters that slide over the input image to extract local features. Each filter captures different features such as edges and corners.

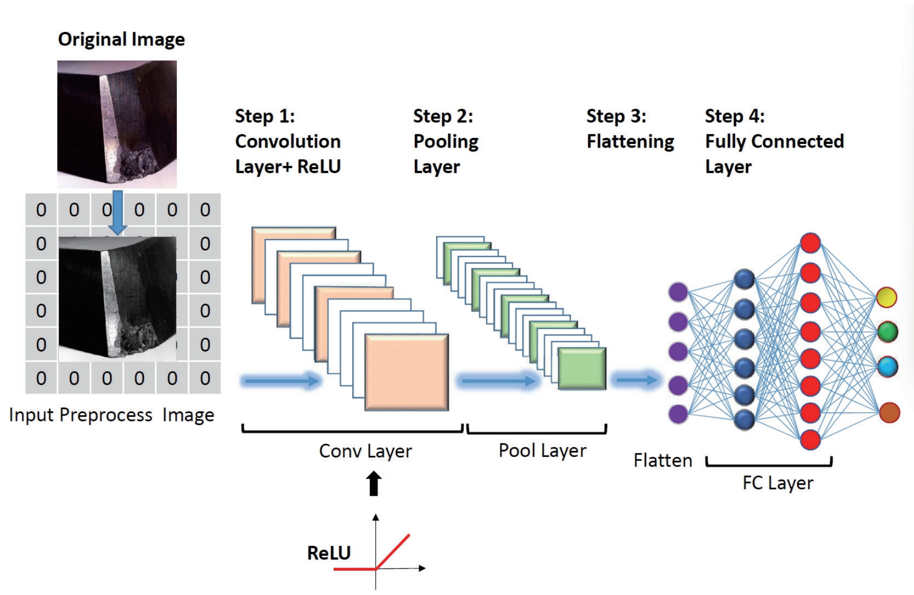

Fig. 6. (Color online) Tool wear CNN framework.

2. Pooling Layers: Pooling layers reduce the dimensionality of feature maps by down sampling, which decreases the number of parameters and computation load while preserving essential features. Common pooling methods include max pooling and average pooling.
3. Fully Connected Layers: After several convolutional and pooling layers, the feature maps are flattened and fed into fully connected layers for classification. These layers function similarly to traditional neural network layers, integrating and classifying the input features.
4. Activation Functions: Activation functions, such as the rectified linear unit (ReLU), introduce nonlinearity into the model, enhancing its representational power. The ReLU function is defined as Eq. (4).
5. Loss Function and Optimization: The loss function (e.g., cross-entropy loss) measures the difference between the predicted and true values. Network weights are updated through backpropagation and optimization algorithms, such as gradient descent, to minimize this loss.

By leveraging these components, CNNs can efficiently process and classify images; this makes them a powerful tool in the field of computer vision.

$$ReLu(x) = \begin{cases} x & \text{if } x > 0 \\ 0 & \text{otherwise} \end{cases} \tag{4}$$

The CNN model architecture utilized in this study comprises the following components: batch normalization, convolutional layers, pooling layers, activation functions, loss function, and fully connected layers.

- Batch Normalization: Applied to the training data, this technique accelerates the training process and enhances model performance.

- Convolutional Layers: These layers perform feature extraction to obtain feature maps from the input images.
- Pooling Layers: These layers are employed for down sampling to significantly reduce computational load. We use max pooling because of its superior performance in practical applications.
- Activation Functions: The ReLU function is used to enhance the network structure, prevent gradient vanishing, and mitigate overfitting.
- Fully Connected Layers: The purpose of these layers is to classify the feature information derived from the convolutional and pooling layers.
- Loss Function: The Softmax function is used to obtain probability values for multiclass classification. The final model prediction categorizes tool wear into three classes representing dull, semidull, and sharp conditions.

This comprehensive architecture leverages each component's strengths to develop a robust model for classifying tool wear levels based on image features.

4. Results

4.1 Experimental equipment

In this study, a high-magnification digital microscope was used throughout the experimental process. Images were captured for 14 worn tool samples and one set of new tool samples, focusing on the three cutting edges subjected to wear during the cutting process. After image acquisition, image preprocessing was performed. The detailed specifications of the experimental hardware are shown in Table 1.

4.2 Experimental environment and interface development

The system processor used in this study is an Intel® Core™ i5-8250U 1.6GHz, paired with an NVIDIA GeForce 2070 dedicated graphics card. The program interface for the tool wear classification model was developed using MATLAB R2020 to design the graphical user interface (GUI), as shown in Fig. 7.

Table 1
Specifications of the digital microscope.

Image sensor	Micron 1.3 m High-resolution CMOS sensor
Microscope lens	Confocal 80X–200X
Light source	White SMD LED × 8 pcs
Hardware interface	USB 2.0
Software	Measurement & Capture
Cable length	1.5 m
Dimensions	31 mm (diameter) × 120 mm (height)
Weight	125 g

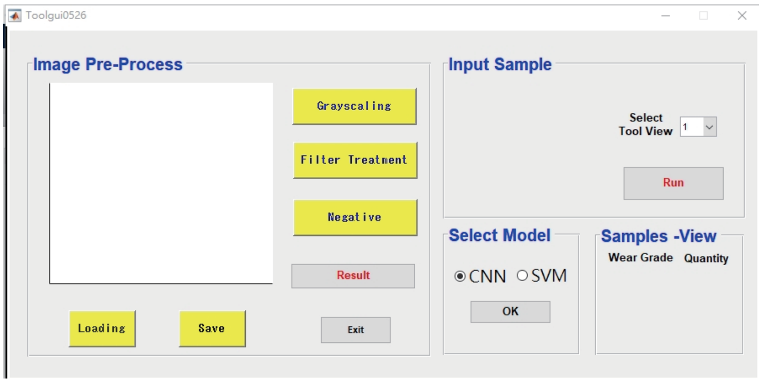

Fig. 7. (Color online) Interface for tool wear classification.

4.3 Experiments

4.3.1 Image preprocessing

According to the methodology described in Sect. 3, we developed a MATLAB-based tool image edge detection process. Step one involves loading the original tool image file and performing edge detection using the Sobel algorithm. The preprocessing results are shown in Fig. 8.

In this study, three different detection methods were employed to calculate the tool wear in three directions. The final wear grade was determined by analyzing the obtained data. Consequently, selecting different directions of samples will display the corresponding wear classification and the number of samples. When there is a need to change the input samples, this can be directly modified through the program interface to expedite the classification process. The practical operation results are shown in Fig. 9.

The initial experiment samples consisted of images capturing the tool tip, secondary relief face, and primary relief face of 15 tools. Images from three angles were obtained for each tool, resulting in a total of 45 tool wear images. These images were classified into three categories based on the severity of wear, ranging from severe to minor. The categories are dull, semi-dull, and sharp, as illustrated in Fig. 10.

On the other hand, data augmentation techniques were employed to fine-tune the existing tool image samples, enhancing the dataset's diversity and improving its generalization capability. In this study, the dataset was expanded using methods such as rotating 30 degrees to the right, rotating 30 degrees to the left, horizontal flipping, vertical flipping, and contrast enhancement. After data augmentation, the tool tip dataset contained 1488 images, the secondary relief face dataset contained 1352 images, and the primary relief face dataset contained 1395 images. The actual effect of data augmentation is shown in Fig. 11.

4.3.2 Parameter settings

In this study, an executable file (EXE) was compiled in the MATLAB environment. When using the system's CNN model, the training parameters can be adjusted in accordance with

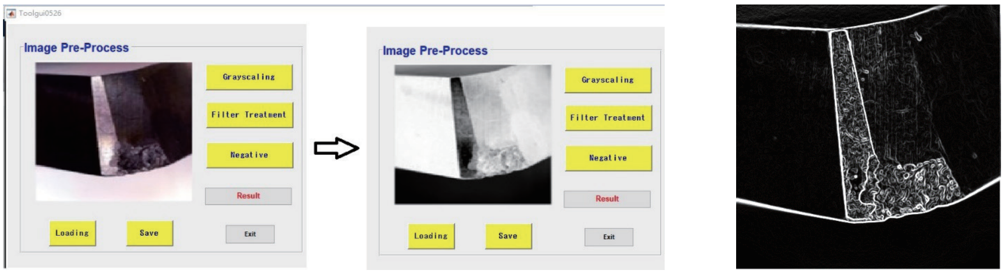

Fig. 8. (Color online) Tool wear image processing results.

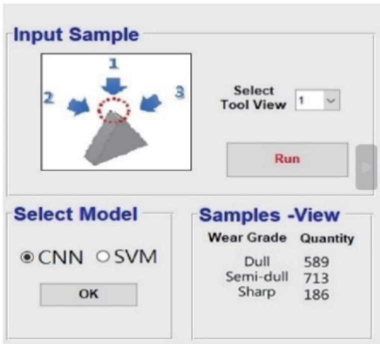

Fig. 9. (Color online) CNN and SVM experimental models.

Fig. 10. (Color online) Three levels of tool wear.

different samples and dataset sizes, as shown in Fig. 12. The parameters that need to be set include the maximum number of epochs, mini batch size, initial learning rate, and validation data frequency.

4.3.2.1 SVM classification

To ensure an equal number of samples for each wear level, we balanced the sample sizes by reducing the number of samples in the other categories to match that in the smallest category. As shown in Fig. 13, the Sharp category, with 186 samples, was the smallest. Therefore, the total

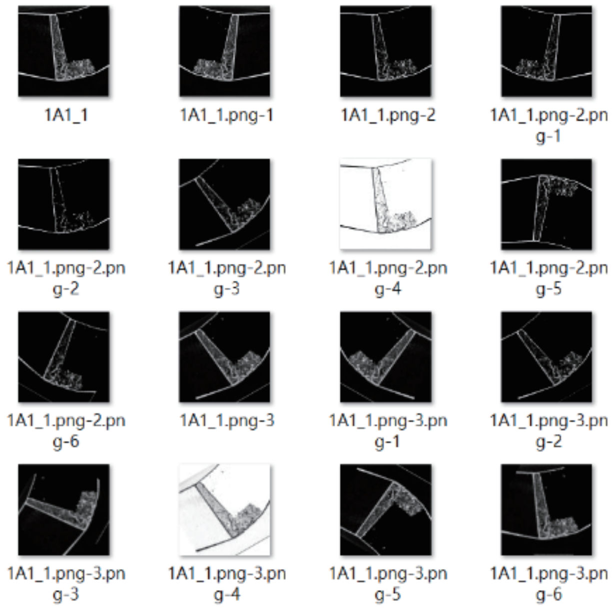

Fig. 11. (Color online) Image data augmentation effect.

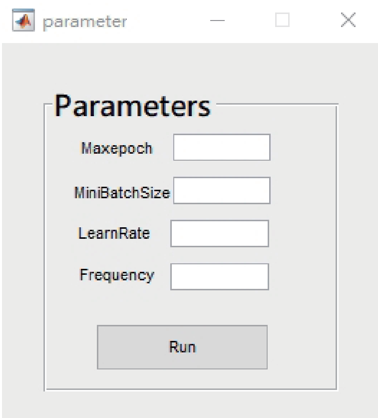

Fig. 12. (Color online) Experimental parameter settings.

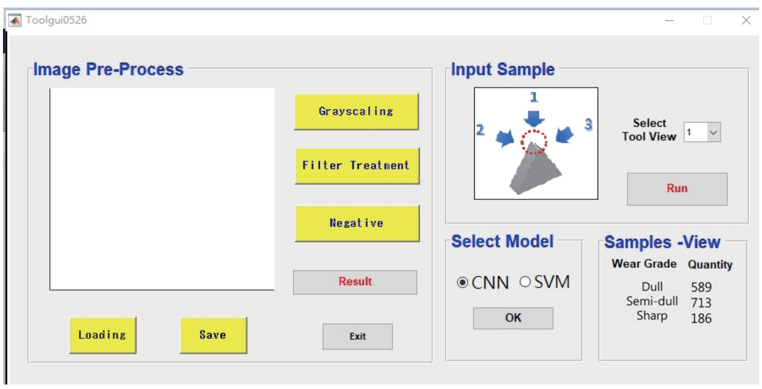

Fig. 13. (Color online) SVM classification model.

sample size was set to 558 (186 × 3) tool wear images. Of these, 70% were randomly selected for training and 30% for testing. The results of this execution are shown in Fig. 14, including the confusion matrix, accuracy, and execution time. Figure 14 shows the prediction results for ten randomly selected test samples; misclassified results are highlighted in red.

The classification accuracies of the SVM model for wear samples at three tool angles (Corner, Minor Flank, and Major Flank) are shown in Fig. 15. It can be observed that the average classification accuracies for the Minor Flank and Major Flank samples are similar, whereas that

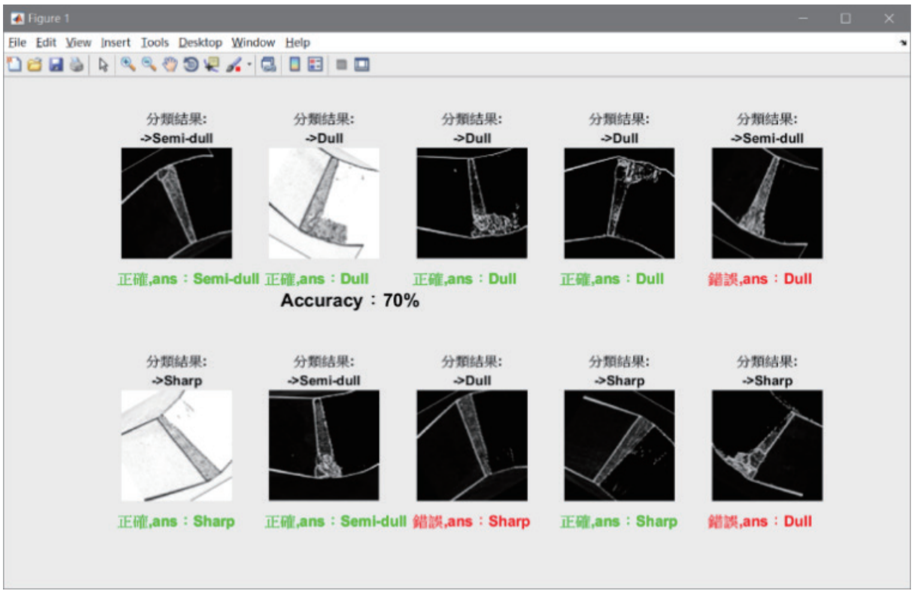

Fig. 14. (Color online) SVM classification model.

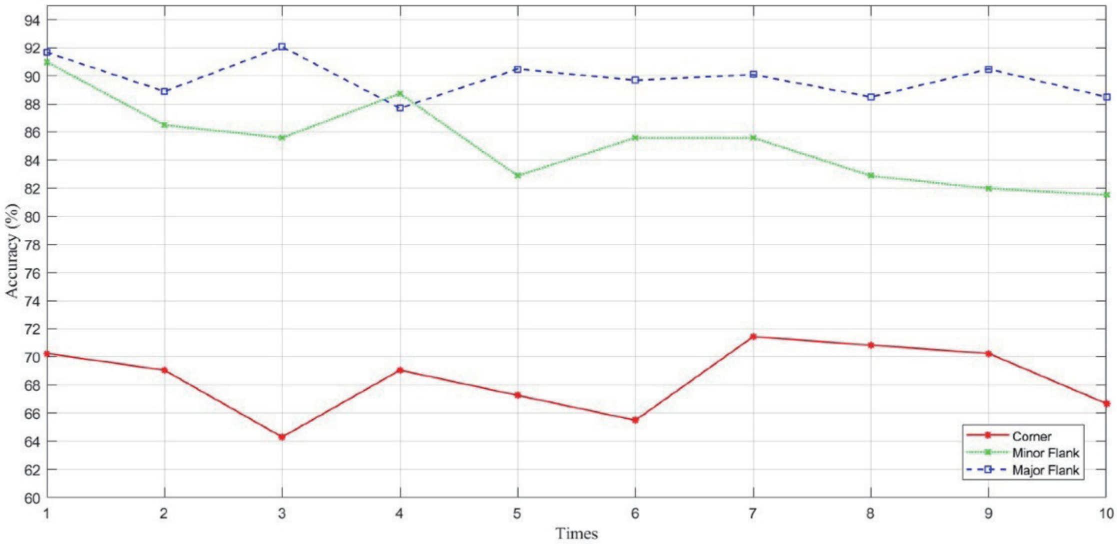

Fig. 15. (Color online) SVM classification model test accuracy.

for the Corner samples is significantly lower. Upon analysis, this decline in accuracy is attributed to the issue of sample size distribution. After balancing the sample sizes to ensure an equal number of samples for each wear level category, the total number of Corner samples was reduced to 558 images; the total number of Minor Flank samples was 744 images; and the total number of Major Flank samples was 837 images. This imbalance led to the SVM model underperforming in classifying the Corner samples compared with the Minor and Major Flank samples.

4.3.2.2 CNN classification

The comparison of classification accuracies of the CNN model for wear samples at the Corner, Minor Flank, and Major Flank tool angles is shown in Fig. 15. The results indicate that despite the sample size differences across the three directions, the CNN model achieved an average accuracy of more than 93% for all three directions. This is in contrast to the SVM model, where the classification accuracy varied significantly under similar conditions, demonstrating a notable difference in classification accuracy between the two models given the same sample sizes. The confusion matrices for the classification results of the CNN and SVM models are presented in Fig. 16, while the classification quality is detailed in Table 2.

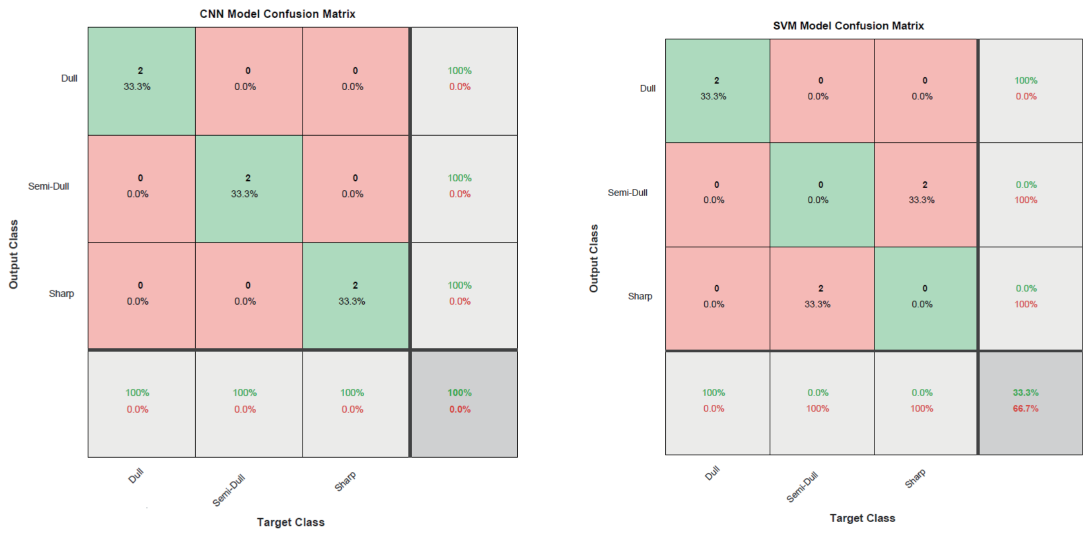

Fig. 16. (Color online) Confusion matrices of CNN and SVM models.

Table 2
CNN and SVM model classification qualities.

Classification Quality Index		SVM Model	CNN Model
Precision	Class=Dull	1.00	1.00
	Class=Semi-dull	0	1.00
	Class=Sharp	0	1.00
Recall	Class=Dull	1.00	1.00
	Class=Semi-dull	0	1.00
	Class=Sharp	0	1.00

5. Conclusions

In this study, machine vision technology was utilized to capture images of wear on the tool tip, minor flank, and major flank. Following image preprocessing, wear measurements were obtained using three techniques: grayscale value, gray-level co-occurrence matrix, and area detection. The measurements were then clustered using the K-means algorithm to determine final wear grades. Tool wear images were subsequently classified using SVM and CNN models.

A comparison of the classification accuracies of the SVM and CNN models revealed that, despite differences in sample sizes across the three directions, the CNN model consistently achieved an average accuracy exceeding 93% in all directions. This performance markedly surpassed that of the SVM model, which exhibited significant variability in accuracy under similar conditions, highlighting the CNN model's superior robustness and reliability in tool wear classification.

Compared with previous research on tool wear, this study was focused specifically on tool wear classification using machine vision, which yielded clear, actionable insights. Concrete, quantifiable results that demonstrate CNN's superior accuracy over SVM were obtained, making CNN highly relevant for practical applications. By directly comparing SVM and CNN, we provide a solid basis for selecting the best AI model for tool wear classification. The emphasis on measurable performance ensures direct applicability to industry needs, and the detailed, step-by-step guide for implementing the classification model further enhances its practical value.

The exploration of the integration of advanced deep learning techniques, such as transfer learning or hybrid models, to further enhance the accuracy and efficiency of tool wear classification is a subject for future research. Additionally, incorporating real-time data from industrial environments could lead to the development of adaptive models that continuously learn and improve from new data. Investigating the use of 3D imaging and more sophisticated image processing algorithms could also provide a more comprehensive analysis of tool wear by capturing subtle wear patterns that 2D images might miss. Finally, expanding the scope to include predictive maintenance systems, where the model not only classifies wear but also predicts future tool performance and lifespan, could significantly benefit industrial applications.

References

1 A. Malakizadi, T. Hajali, F. Schulz, S. Cedergren, J. Ålgårdh, R. M'Saoubi, E. Hryha, and P. Krajnik: Int. J. Mach. Tools Manuf. **171** (2021) 103814. https://doi.org/10.1016/j.ijmachtools.2021.103814

2 L. Hao, L. Bian, N. Gebraeel, and J. Shi: IEEE Trans. Autom. Sci. Eng. **14** (2017) 1211. https://doi.org/10.1109/TASE.2015.2513208

3 J. Karandikar, T. McLeay, S. Turner, and T. Schmitz: Int. J. Adv. Manuf. Technol. **77** (2015) 1613. https://doi.org/10.1007/s00170-014-6560-6

4 Y. Zhou and W. Xue: Int. J. Adv. Manuf. Technol. **96** (2018) 2509. https://doi.org/10.1007/s00170-018-1768-5

5 R. Singh, A. Gehlot, S. V. Akram, L. R. Gupta, M. K. Jena, C. Prakash, S. Singh, and R. Kumar: Sustainability **13** (2021) 7327. https://doi.org/10.3390/su13137327

6 M. H. Abidi, M. K. Mohammed, and H. Alkhalefah: Sustainability **14** (2022) 3387. https://doi.org/10.3390/su14063387

7 C. Chen, H. Fu, Y. Zheng, F. Tao, and Y. Liu: J. Manuf. Syst. **71** (2022) 581. https://doi.org/10.1016/j.jmsy.2023.10.010

8 S. Shurrab, A. Almshnanah, and R. Duwairi: 12th Int. Conf. Inf. Commun. Syst. (IEEE 2021) 24–26. https://doi.org/10.1109/ICICS52457.2021.9464580
9 Y. Lei, B. Yang, X. Jiang, F. Jia, and A. K. Nandi: Mech. Syst. Signal Process. **138** (2020) 106587. https://doi.org/10.1016/j.ymssp.2019.106587
10 R. Munaro, A. Attanasio, and A. D. Prete: J. Manuf. Mater. Process. **7** (2023) 129. https://doi.org/10.3390/jmmp7040129
11 G. Serin, B. Sener, A. Ozbayoglu, and H. O. Unver: J. Adv. Manuf. Technol. **109** (2020) 723. https://doi.org/10.1007/s00170-020-05449-w
12 J. Wang, J. Xie, R. Zhao, L. Zhang, and L. Duan: Rob. Comput. Integr. Manuf. **45** (2017) 47. https://doi.org/10.1016/j.rcim.2016.05.010
13 P. J. Bagga, M. A. Makhesana, H. D. Patel, and K. M. Patel: Mater. Today Proc. **44** (2021) 1549. https://doi.org/10.1016/j.matpr.2020.11.770
14 M. A. Giovanna, G. Terrazas, and S. Ratchev: J. Adv. Manuf. Technol. **104** (2019) 3647. https://doi.org/10.1007/s00170-019-04090-6
15 W. Cai, W. Zhang, X. Hu, and Y. Liu: J. Intell. Manuf. **31** (2020) 1497. https://doi.org/10.1007/s10845-019-01526-4
16 Z. C. Lipton: Commun. ACM **61** (2018) 36. https://doi.org/10.1145/3233231
17 J. P. Davim and V. P. Astakhov: Machining: Fundamentals and Recent Advances, J. P. Davim Eds. (Springer, 2008) pp. 29–57.
18 R. G. Silva, R. L. Reuben, K. J. Baker, and S. J. Wilcox: Mech. Syst. Signal Process. **12** (1998) 319. https://doi.org/10.1006/mssp.1997.0123
19 D. A. Dornfeld and E. Kannatey-Asibu: Int. J. Mech. Sci. **22** (1980) 285. https://doi.org/10.1016/0020-7403(80)90029-6
20 W. Y. Bao and I. N. Tansel: In. J. Mach. Tools Manuf. **40** (2000) 2193. https://doi.org/10.1016/S0890-6955(00)00056-0
21 W. Rmili, A. Ouahabi, R. Serra, and R. Leroy: Measurement **77** (2016) 117. https://doi.org/10.1016/j.measurement.2015.09.010
22 K. Vacharanukul and S. Mekid: Measurement **38** (2005) 204. https://doi.org/10.1016/j.measurement.2005.07.009
23 K. Zhu and X. Yu: Mech. Syst. Signal Process. **93** (2017) 80. https://doi.org/10.1016/j.ymssp.2017.02.004
24 U. Župerl, K. Stepien, G. Munđar, and M. Kovačič: Processes **10** (2022) 671. https://doi.org/10.3390/pr10040671
25 T. Mohanraj, J. Yerchuru, H. Krishnan, R. S. Nithin Aravind, and R. Yameni: Measurement **173** (2021) 108671. https://doi.org/10.1016/j.measurement.2020.108671
26 Z. Li, R. Liu, and D. Wu: J. Manuf. Process. **48** (2019) 66. https://doi.org/10.1016/j.jmapro.2019.10.020
27 F. Kara: Mater. Test. **59** (2017) 903. https://doi.org/10.3139/120.111085
28 R. Dastres and M. Soori: Int. J. Eng. Res. **19** (2022) 1. https://hal.science/hal-03367778
29 D. Y. Pimenov, A. Bustillo, S. Wojciechowski, V. S. Sharma, M. K. Gupta, and M. Kuntoğlu: J. Intell. Manuf. **34** (2022) 2079. https://doi.org/10.1007/s10845-022-01923-2
30 J. Wang, J. Xie, R. Zhao, L. Zhang, and L. Duan: Rob. Comput. Integr. Manuf. **45** (2017) 47. https://doi.org/10.1016/j.rcim.2016.05.010
31 G. Xu, H. Zhou, and J. Chen: Eng. Appl. Artif. Intell. **74** (2018) 90. https://doi.org/10.1016/j.engappai.2018.05.007
32 F. Aghazadeh, A. Tahan, and M. Thomas: Int. J. Adv. Manuf. Technol. **98** (2018) 3217. https://doi.org/10.1007/s00170-018-2420-0
33 Q. Chen, Q. Xie, Q. Yuan, H. Huang, and Y. Li: Symmetry **11** (2019) 1233. https://doi.org/10.3390/sym11101233
34 L. Li, S. Chen, M. Deng, and Z. Gao: Grain Oil Sci. Technol. **5** (2022) 44. https://doi.org/10.1016/j.gaost.2021.12.001
35 Y. H. Tsai, N. Y. Lyu, S. Y. Jung, K. H. Chang, J. Y. Chang, and C. T. Sun: Proc. IEEE Int. Conf. Adv. Intell. Mechatronics (China, 2019) 103. https://doi.org/10.1109/AIM.2019.8868602
36 N. Iqbal, R. Mumtaz, U. Shafi, and SMH Zaidi: PeerJ Comput. Sci. **7** (2021) e536. https://doi.org/10.7717/peerj-cs.536
37 N. Agarwal, V. N. Balasubramanian, and C. V. Jawahar: Pattern Recognit. Lett. **112** (2018) 184. https://doi.org/10.1016/j.patrec.2018.06.034
38 N. Laopracha, K. Sunat, and S. Chiewchanwattana: IEEE Access **7** (2019) 20894. https://doi.org/10.1109/ACCESS.2019.2893320

About the Authors

Yung-Hsiang Hung received his Ph.D. degree in industrial engineering and management from National Chiao-Tung University, R.O.C., in 2002. He is a professor in the Department of Industrial Engineering and Management at National Chin-Yi University of Technology, Taiwan, R.O.C. His main research interests are in statistical process control, service quality management, process capability analysis, semiconductor manufacturing management, and process parameter optimization design. (hys502@ncut.edu.tw)

Mei-Ling Huang received her M.S. and Ph.D. degrees in industrial engineering from the University of Wisconsin–Madison and National Chiao-Tung University, respectively. She is now affiliated with the Department of Industrial Engineering & Management at National Chin-Yi University of Technology. Her research interests include quality management, quality engineering, data mining, and medical diagnosis. (huangml@ncut.edu.tw)

Wen-Pai Wang received his M.S. and Ph.D. degrees in industrial engineering from Kansas State University and National Chiao-Tung University, respectively. He is currently a professor in the Department of Industrial Engineering and Management at National Chin-Yi University of Technology. His research interests are in fuzzy set theory, product development and operations/ manufacturing management, and decision theory. (wangwp@ncut.edu.tw)

Hsiao-Dan Hsieh received her M.S. degree from the Department of Industrial Engineering and Management, National Chin-Yi University of Technology, Taichung City, Taiwan, in 2019. Her research interests are in deep learning and image recognition. (Huliouo@gmail.com)